Ce/Gd Co-doping in NiFe LDH Engineered Oxygen Vacancies for Enhanced Oxygen Evolution

Xiaobing Bao,[a] Junfeng Wang,[a] Yang Yang,[a] Qiqi Liu,[a] Xiaoyong Fan,[a] Shanjun Mao[b], Yutong Gong*[c] and Lei Gou*[a]

Experimental section

Preparation of catalysts

NiFe LDH: Firstly, the trimmed Ni foam (NF) of 2.0 cm * 2.0 cm was placed in 1.0 M hydrochloric acid for ultrasonic treatment for 30 min to wipe off oxides on the surface. Then, the NF was cleaned in acetone, deionized water, and ethanol for 10 min, respectively. The treated NF was dried at 80 ℃ for 4 h. The NiFe-LDH was synthesized by one-step hydrothermal method. Here, 0.9 mmol $Ni(NO_3)_2{\cdot}6H_2O$, 0.3 mmol $Fe(NO_3)_3{\cdot}9H_2O$, 6 mmol CH_4N_2O, and 4 mmol NH_4F were added to 30 mL deionized water and agitated at room temperature for 10 min. The treated NF was immersed in the mixed solution and transferred into a 50 ml reactor treated at 120 ℃ for 8 h. The obtained NiFe LDH was cleaned with deionized water and ethanol three times, and then dried in the oven at 80 ℃ for 4 h to acquire the final catalyst.

Ce, Gd-NiFe LDH: The preparation method of rare earth doped NiFe-LDH is similar to that of NiFe-LDH, except for the additional addition of rare earth salt into the mixed solution. Notably, the amount of $Ni(NO_3)_2{\cdot}6H_2O$ remains the same, and the molar amount of ferric nitrate decreases accordingly with the addition amount of rare earth salts ($Ce(NO_3)_3{\cdot}6H_2O$ and $Gd(NO_3)_3{\cdot}6H_2O$). Correspondingly, the synthesis of single-element doped samples (Ce-NiFe LDH and Gd-NiFe LDH) involved the addition of only the specific precursor salt. In order to study the effect of Ce and Gd content on activity, the addition amount of Ce and Gd added is changed sequentially, and the corresponding samples are recorded as x y-NiFe LDH, wherein x=0.5, 1.0, and 1.5, respectively; y=Ce or Gd.

Structure characterization

The morphology and structure of the prepared sample were obtained by scanning electron

microscopy (SEM, JEOL JSM-7100F). The crystal structure of the sample was characterized by X-ray diffraction (XRD), radiation source: Cu-Kα, electromagnetic wave wavelength: 0.15406 nm. The scanning range: 2θ = 10° ~ 80°. The distribution of elements was analyzed by energy dispersive X-ray spectrometer (EDX). Fourier transform infrared spectroscopy (FT-IR) is obtained by a Fourier transform infrared spectrometer named ThermoScientificNicoletS5, in which KBr pressing technique is used in the measurement of FT-IR. X-ray photoelectron spectroscopy (XPS) is tested by an X-ray photoelectron spectrometer. Among them, the vacuum of the analysis chamber is 8 ×l0−10Pa, the excitation source is Alka line ray (hv = 1486.6 eV), the filament current is 16 mA, the working voltage is 12.5 kV, and the charge is corrected according to the energy standard of C 1s = 284.80 eV binding energy. The EPR (Bruker EMXnano) was used to recognize O_v of Ce, Gd-NiFe LDH with a power of 100 mW, a scanning range of -100~5000 G, and a magnetic field resolution of 4 μG. The Ce and Gd contents of Ce, Gd-NiFe LDH were determined by inductively coupled plasma-optical emission spectroscopy (ICP-OES, Agilent 725, USA).

Electrochemical testing

All the electrochemical measurements were performed using a CHI 660F electrochemical workstation. All the materials were cut into 1 cm × 1 cm and used as the working electrode directly. The Hg/HgO and graphite rod were used as the reference electrode and the counter electrode, respectively. The test solution is 1.0 M KOH (pH = 13.8). The catalysts were subjected to cyclic voltammetry (CV) for hundreds of cycles to reach a steady state before routine testing. Linear sweep voltammetry (LSV) curves were recorded from high to low potential with a scan rate of 5 mV s^{-1} with iR-compensation. The double layer capacitance (C_{dl}) was performed in the non-Faradaic potential interval with gradient scan rates. Electrochemical impedance spectroscopy (EIS) was carried out in the frequency range from 10^5 Hz to 10^{-2} Hz at an amplitude of 5 mV. Chronopotentiometry curves were recorded at 10 mA cm^{-2} to study the stability of the catalysts. The actual pH of all electrolytes is measured using a calibrated high-precision pH meter (METTLER TOLEDO, SD20). The measured potential is corrected by the standard reversible hydrogen electrode potential, that is, $E_{RHE} = E_{Hg/HgO} + 0.098 + 0.059 \times pH$. The overpotential (η) is calculated according to the formula $\eta = E_{RHE}-1.23$.

DFT Calculations

Density functional theory (DFT) calculations were carried out with the Vienna Ab initio Simulation Package (VASP)[1]. The projector-augmented wave (PAW) method was utilized to characterize electron–ion interactions, and the exchange–correlation functional was treated within the generalized gradient approximation (GGA) using the Perdew–Burke–Ernzerhof (PBE) functional[2]. The electronic wavefunctions were expanded in a plane-wave basis set with a kinetic energy cutoff of 520 eV. Geometry optimization was carried out via the conjugate gradient algorithm, where convergence thresholds were set to 10^{-5} eV for the total energy and 0.03 eV·Å^{-1} for the interatomic forces. A 2×4×1 k-point mesh from the Gamma-centered scheme was adopted for calculations.

Periodic slab models were constructed from 2×1×1 supercells of the NiFe-LDH(001) surface. A vacuum spacing of 20 Å was introduced along the direction normal to the surface to decouple periodic replicas. To examine the influence of Ce and Gd doping on V_{OH} formation, two surface Ni atoms were replaced by one Ce atom and one Gd atom, respectively. To mimic the constraints imposed by the underlying bulk material, the two bottom layers were fixed during the optimizing process, and the surface layers were allowed to relax. The formation energy for an oxygen vacancy (E_{OV}) was calculated by removing an OH from the parental structure as follows:

$$E_{OV} = E_{defect} + E_{OH} - E_{perfect} \quad \#$$

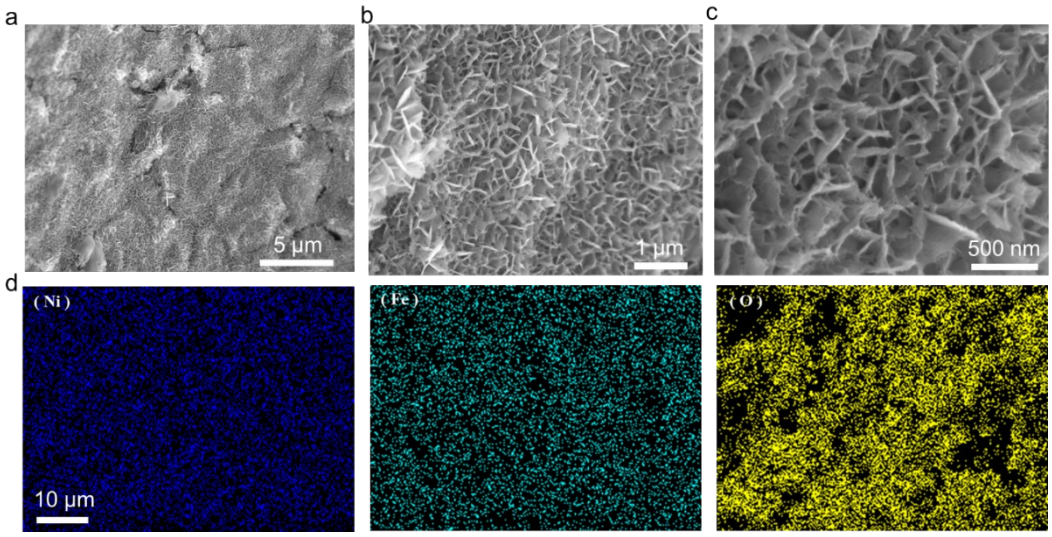

Figure S1. (a-c) SEM of NiFe LDH catalyst and (d) the corresponding EDS images of Ni, Fe, and O elements

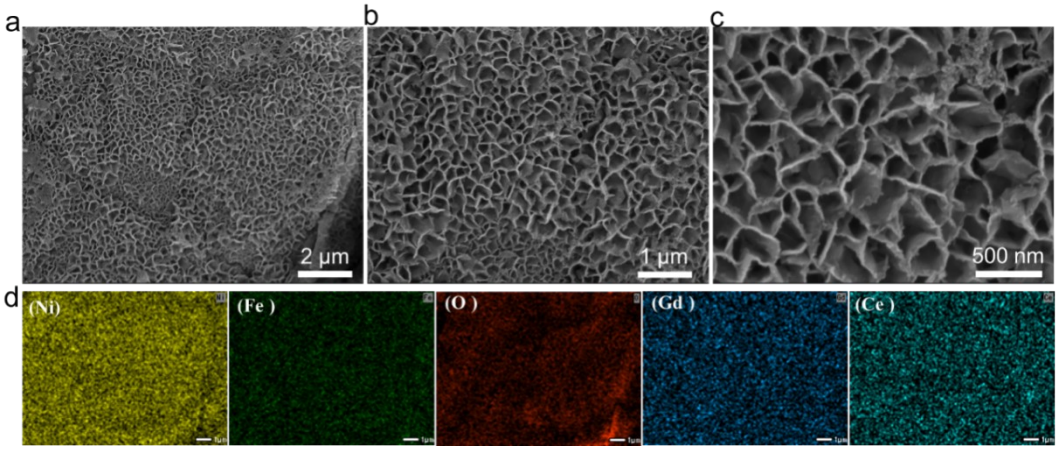

Figure S2. (a-c) SEM images of Ce, Gd-NiFe LDH catalyst and (d) the corresponding EDS images of Ni, Fe, O, Ce, and Gd elements

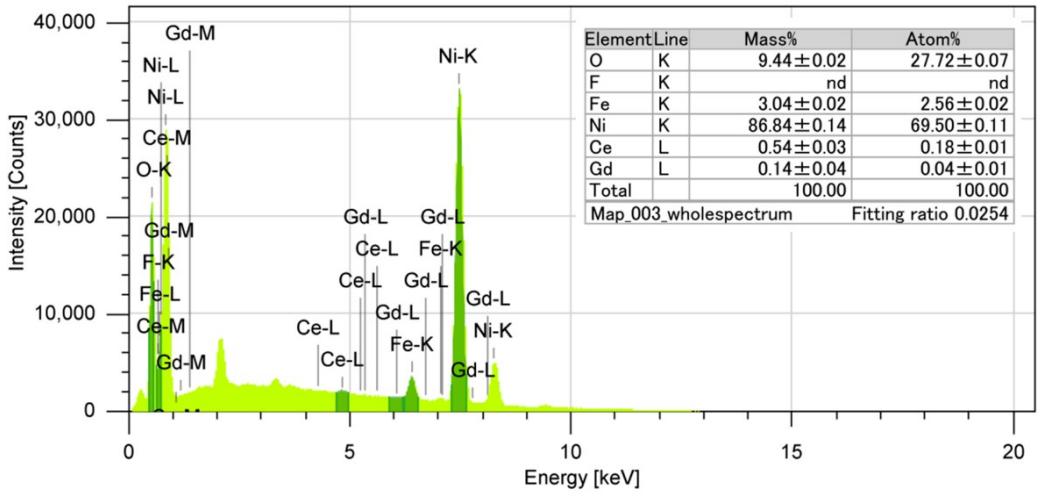

Figure S3. Elemental contents of Ce, Gd-NiFe LDH catalyst based on the EDS

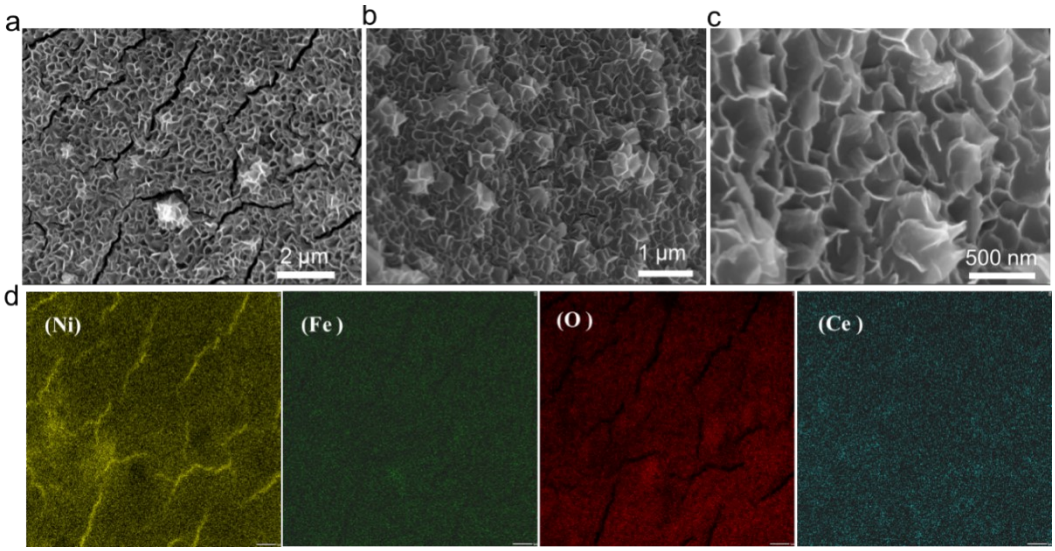

Figure S4. (a-c) SEM images of Ce-NiFe LDH catalyst and (d) the corresponding EDS images of Ni, Fe, O, and Ce elements

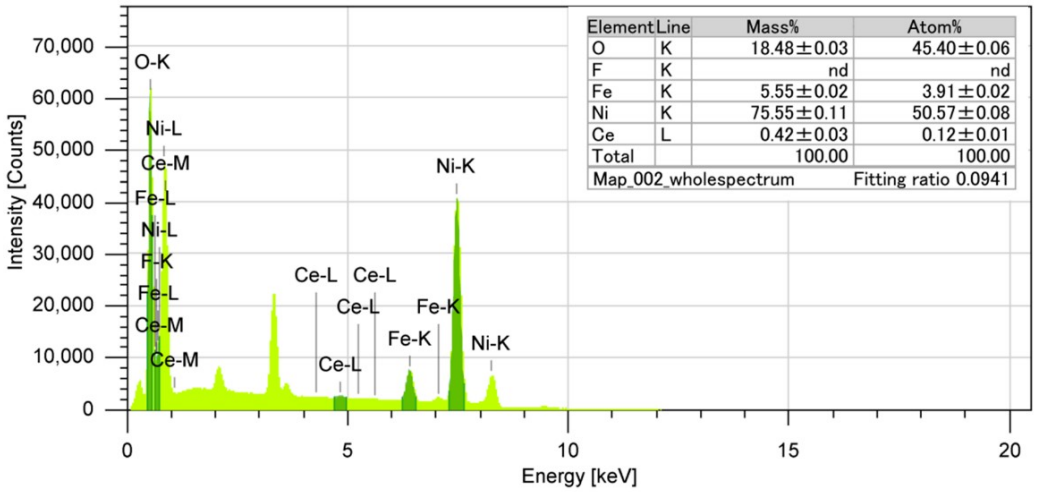

Figure S5. Elemental contents of Ce-NiFe LDH catalyst based on the EDS

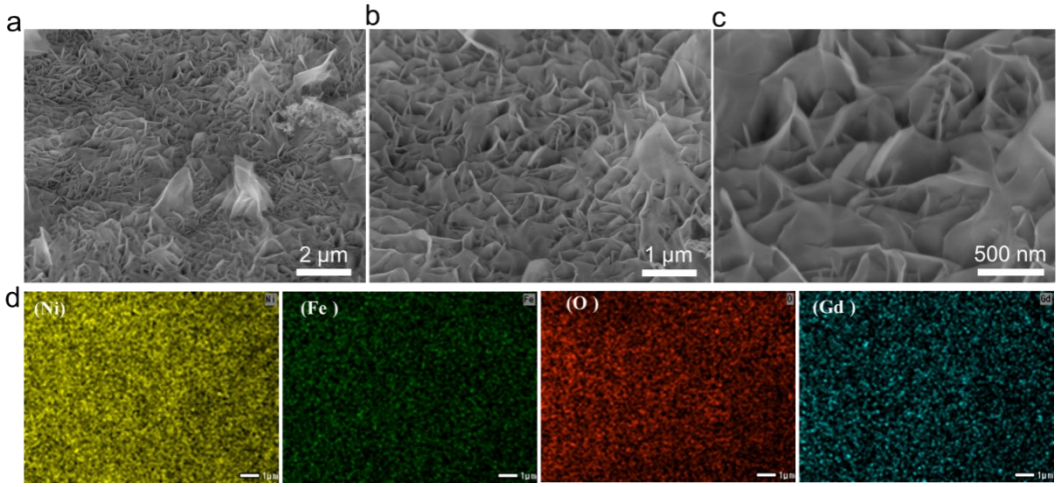

Figure S6. (a-c) SEM images of Gd-NiFe LDH and (d) the corresponding EDS images of Ni, Fe, O, and Gd elements

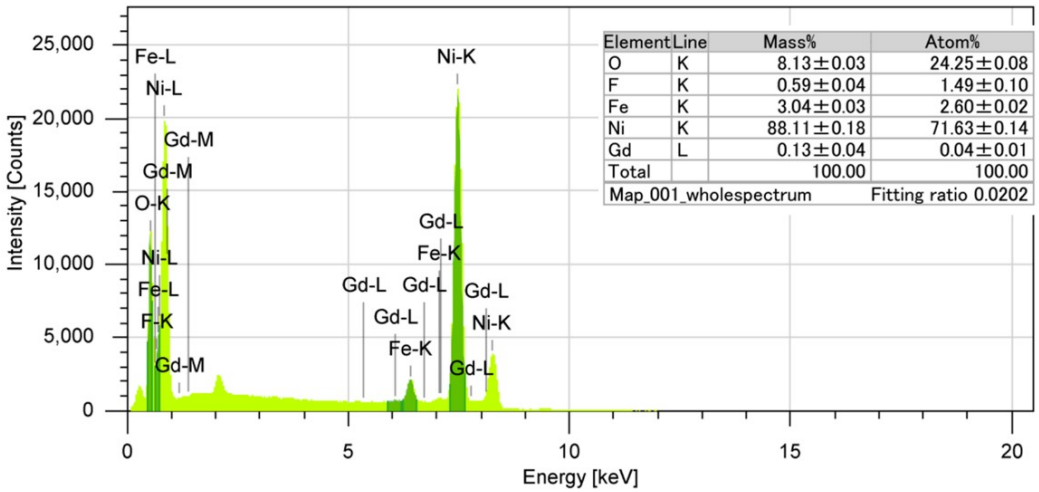

Element	Line	Mass%	Atom%
O	K	8.13±0.03	24.25±0.08
F	K	0.59±0.04	1.49±0.10
Fe	K	3.04±0.03	2.60±0.02
Ni	K	88.11±0.18	71.63±0.14
Gd	L	0.13±0.04	0.04±0.01
Total		100.00	100.00
Map_001_wholespectrum			Fitting ratio 0.0202

Figure S7. Elemental contents of Gd-NiFe LDH based on the EDS

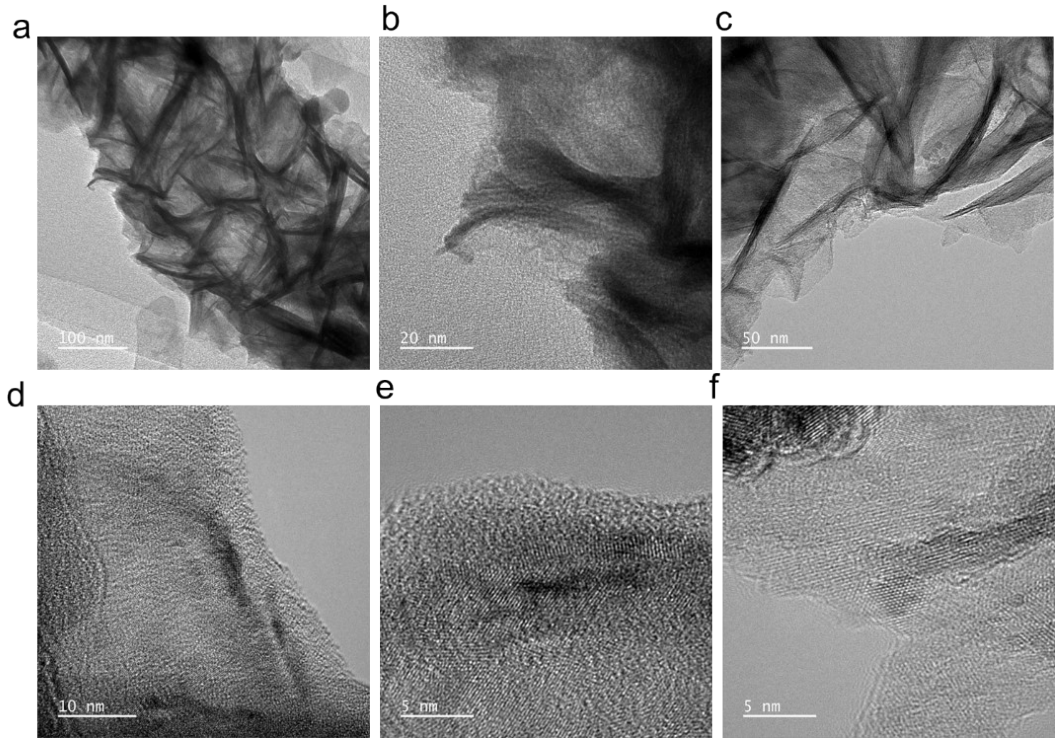

Figure S8. HRTEM images of Ce, Gd-NiFe LDH

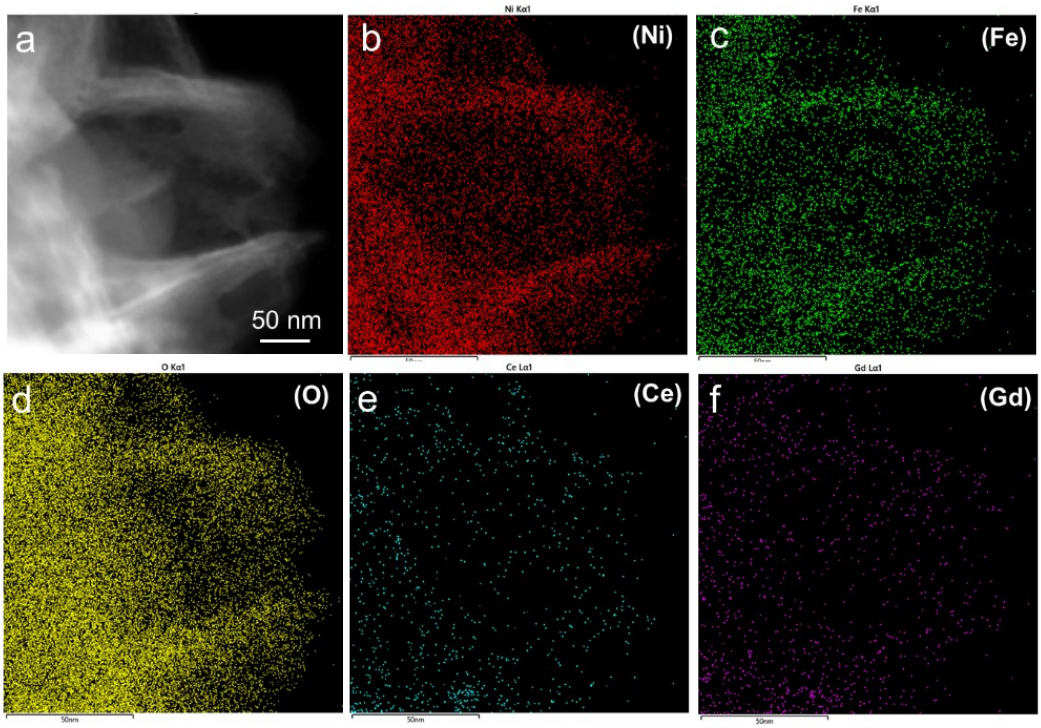

Figure S9. HAADF-STEM image (a) and corresponding EDS elemental mappings (b-f) of Ce, Gd-NiFe LDH

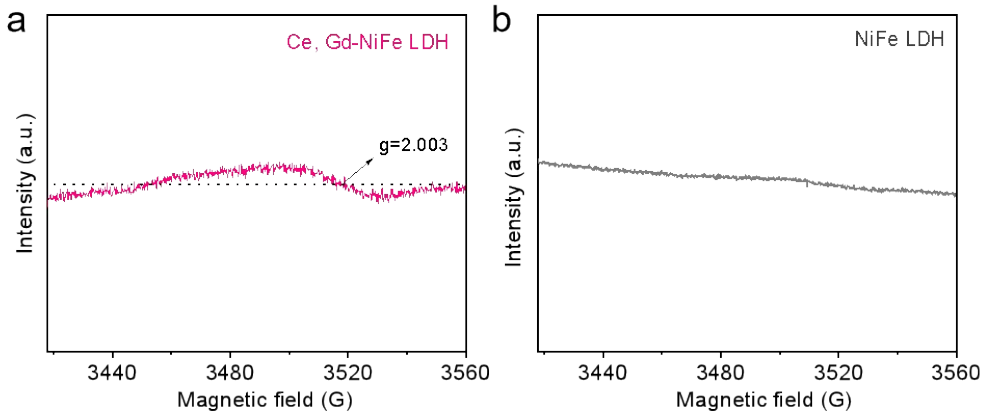

Figure S10. EPR spectra of Ce,Gd-NiFe LDH (a) and NiFe LDH (b)

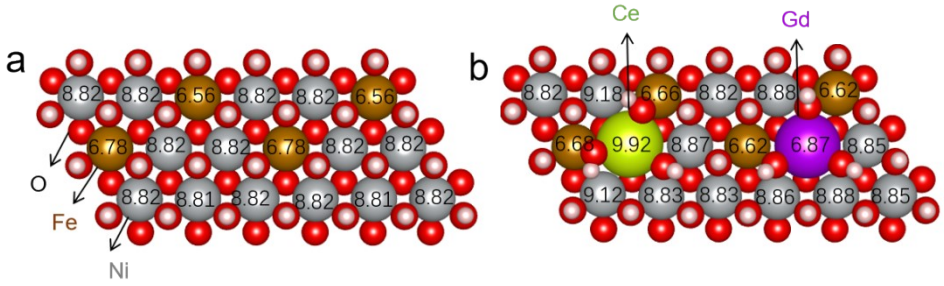

Figure S11. Bader charge analysis of pristine NiFe LDH (a) and doped NiFe LDH (b)

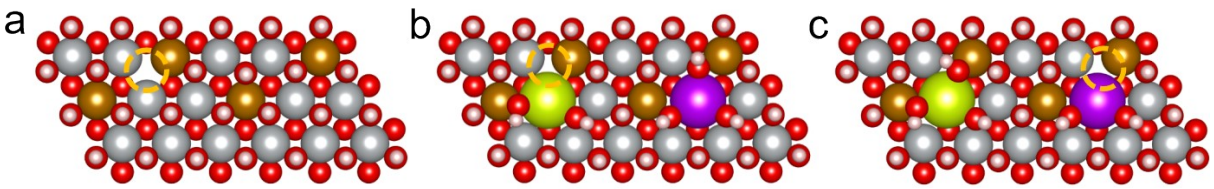

Figure S12. Configurations of NiFe LDH (a) and Ce, Gd-NiFe LDH (b, c) with one oxygen vacancy at different sites (the formation energies of oxygen vacancy are summarized in Table S2)

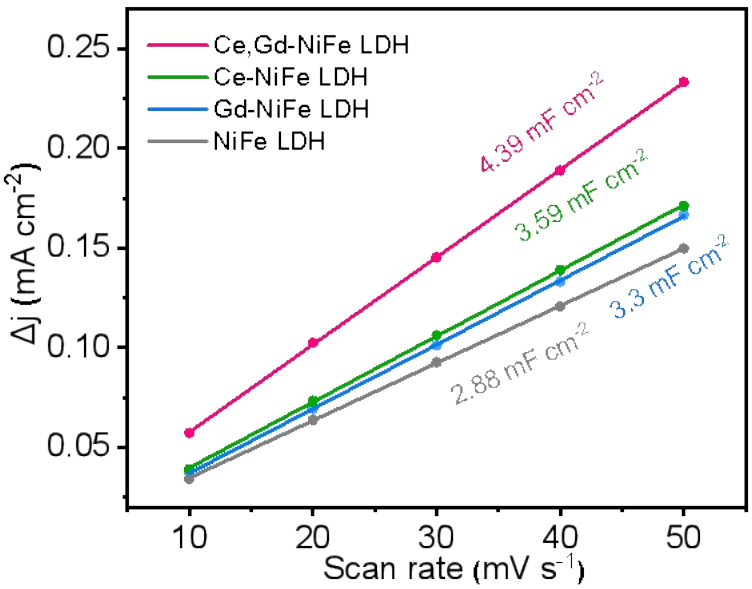

Figure S13. Plots of $\triangle j$ vs. scanning rates for determination of C_{dl}

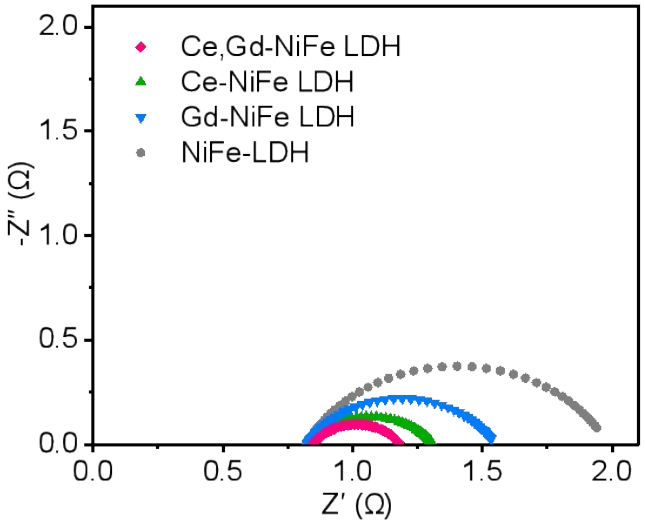

Figure S14. Nyquist plots measured at 1.45 V (vs. RHE)

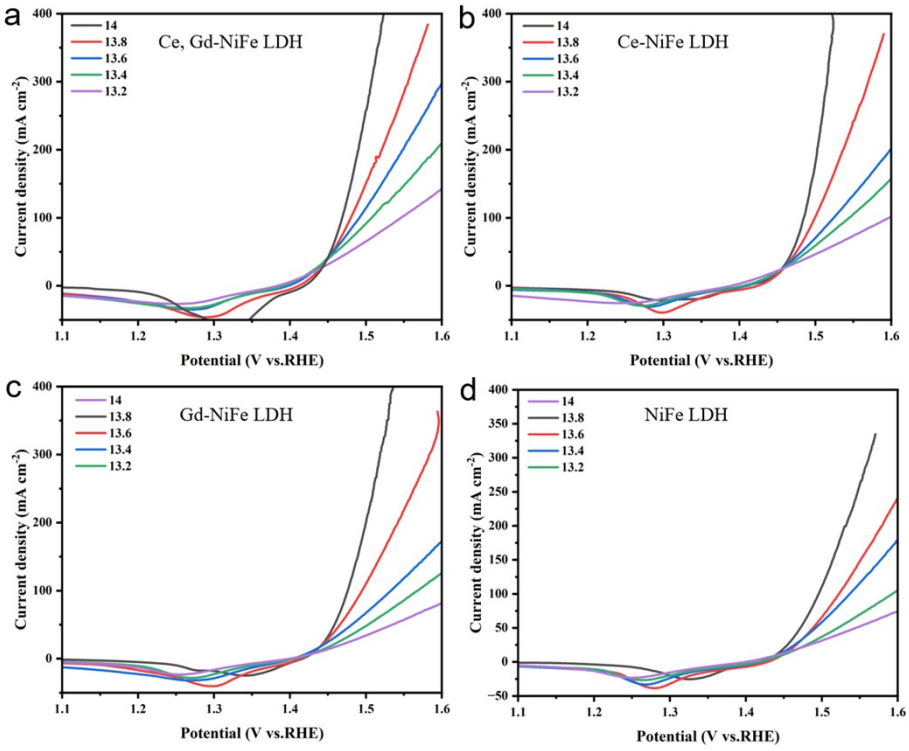

Figure S15. Current density–pH profile of the (a) Ce, Gd-NiFe LDH, (b) Ce-NiFe LDH, (c) Gd-NiFe LDH, and (d) NiFe LDH in KOH electrolytes. (pH: 13.2 ~ 14.0)

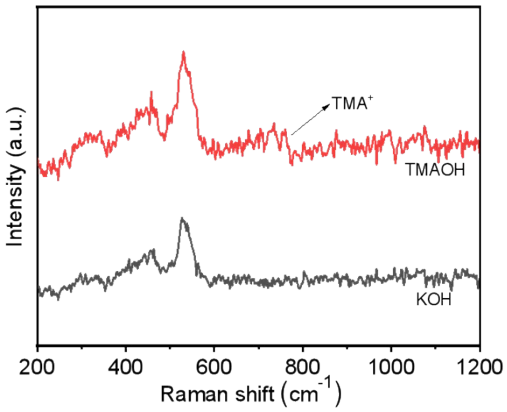

Figure S16. Raman spectra of Ce, Gd-NiFe LDH after OER in 1.0 M KOH and 1.0 M TMAOH, respectively

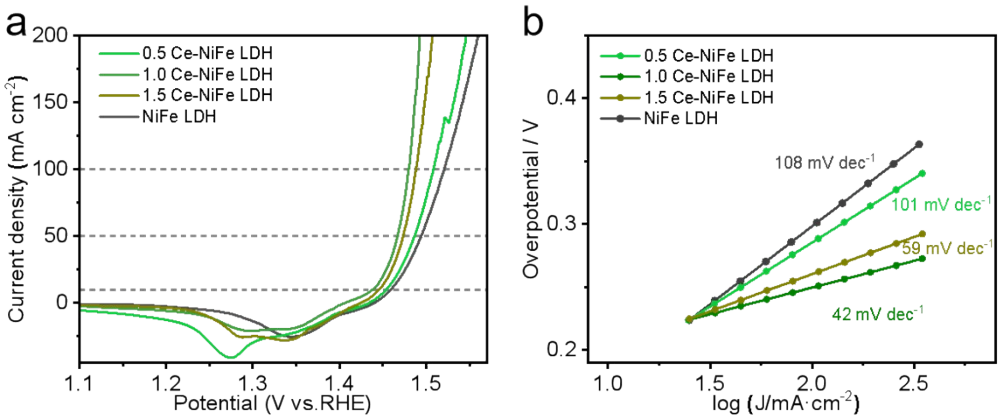

Figure S17. (a) OER polarization curves of Ce-NiFe LDH with different Ce contents; (b) Tafel plots derived from the LSV measurements

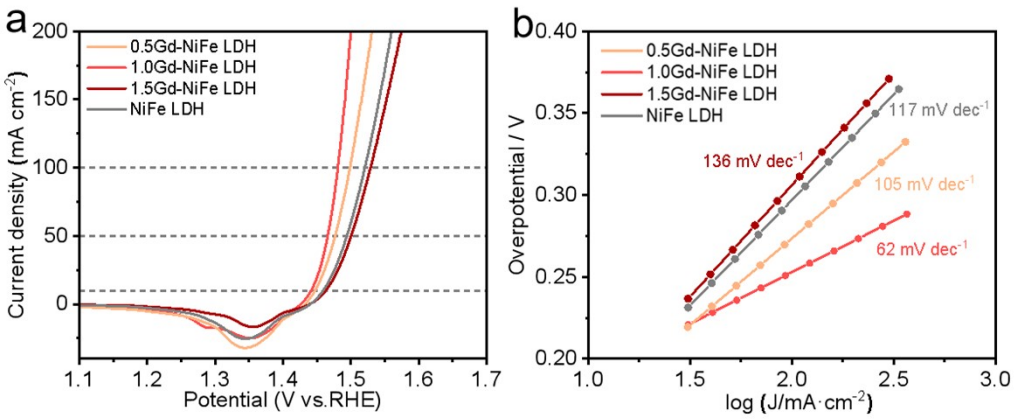

Figure S18. (a) OER polarization curves of Gd-NiFe LDH with different Gd contents; (b) Tafel plots derived from the LSV measurements

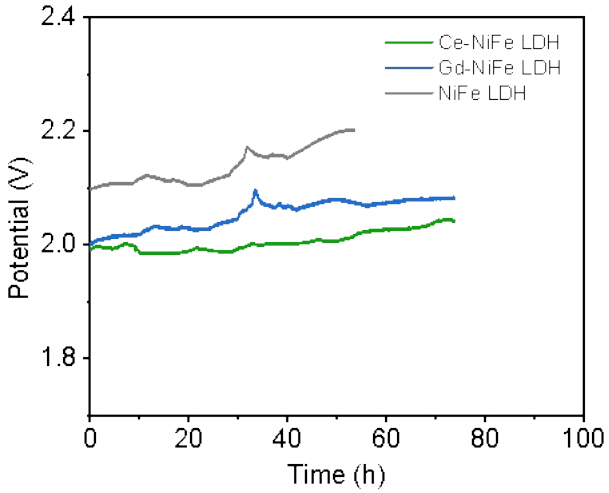

Figure S19. Chronoamperometric curves at 200 mA cm^{-2} of Ce-NiFe LDH, Gd-NiFe LDH, and NiFe LDH.

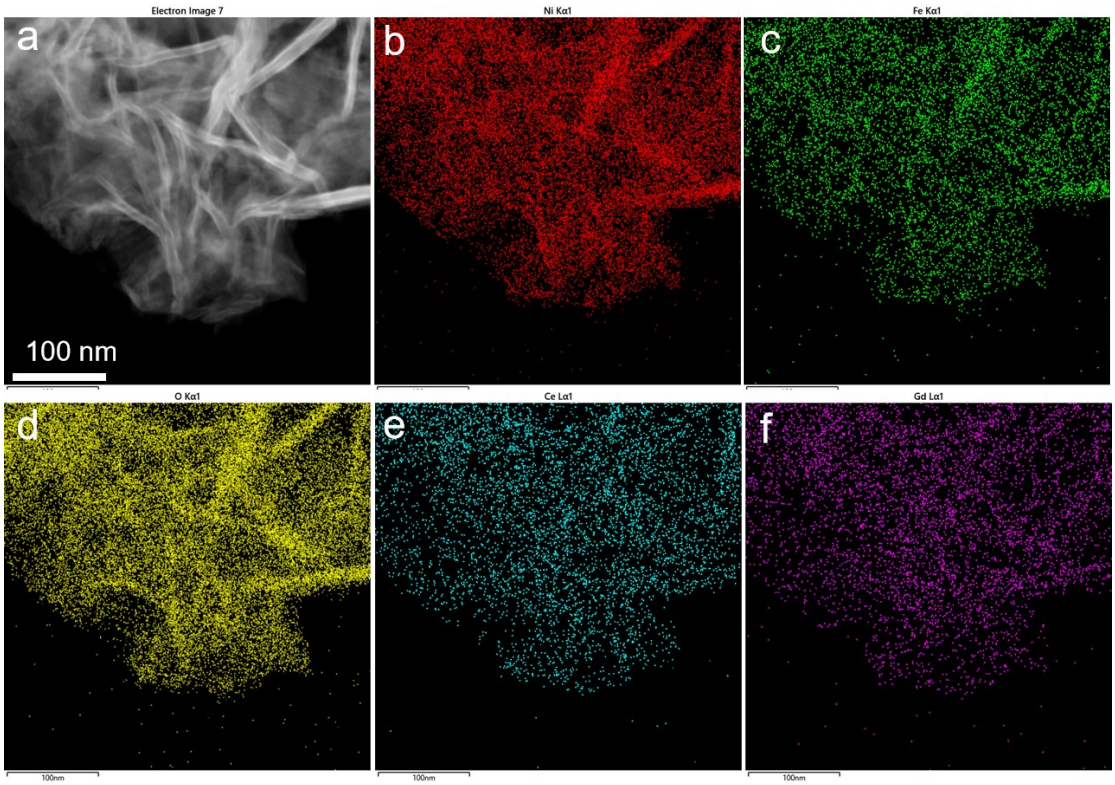

Figure S20. HAADF-STEM image and corresponding EDS elemental mapping of Ce, Gd-NiFe LDH after stability test.

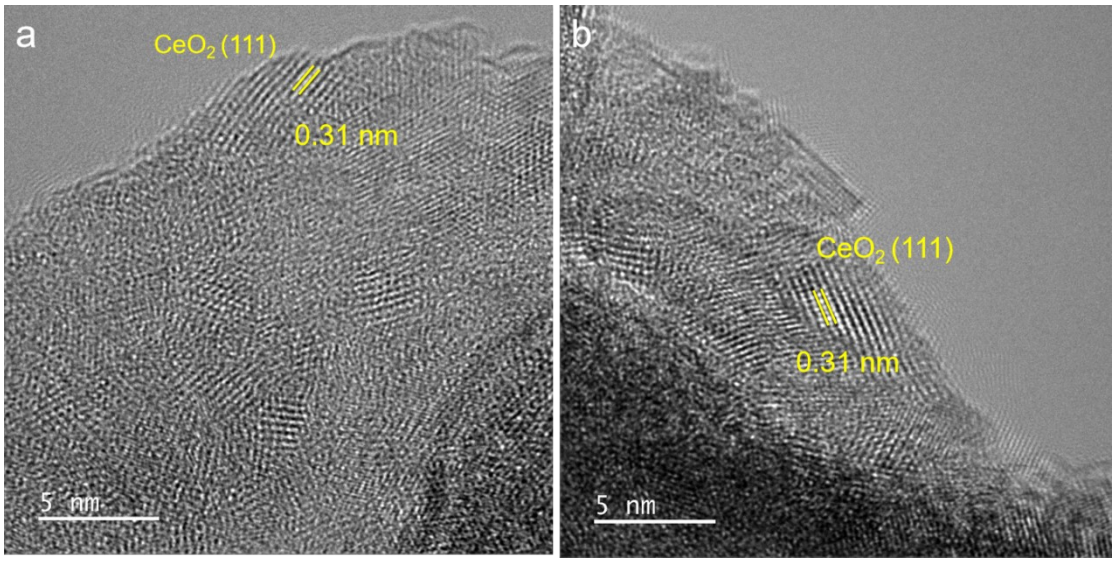

Figure S21. HRTEM images of Ce, Gd-NiFe LDH after stability test.

Table S1. OER performances of Ce, Gd-NiFe LDH and other state-of-the-art OER self-supported electrodes in 1.0 M KOH

Electrodes	η_{10} (mV)	η_{100} (mV)	Reference
Ce, Gd-NiFe LDH	198	-	This work
Pt_{SA}-Mn,Fe-Ni LDHs	288	-	ACS Nano, 2024, 18, 16222-16235
NiFe-S-V_s/NF	213	-	Appl. Surf. Sci., 2019, 484, 1010-1018.
Ir@NiFe-MOF	213	-	Adv. Sci., 2024, 11, 2401780.
NiFe-LDH/Ni_4Mo	192.5	-	Angew. Chem. Int. Ed., 2025, 64, e202413250.
P-(Ni,Fe)O_xH_y	221	-	Nano Res., 2018, 11, 1294-1300.
Ni(Fe)OOH-FeS_x	220	-	Nature Commun., 2020, 11, 5075.
Fe-CoNi LDHs	261	-	Appl. Surf. Sci., 2021, 565, 150506.
Mo-NiS@NiFe LDH/NF	184	-	J. Colloid Interface Sci., 2023, 641, 277-288.
NiFe V fiber	269	-	Angew. Chem. Int. Ed., 2022, 61 c202115331.
Ta-NiFe LDH	280	-	Chem. Eng. J., 2021, 403, 126297.
S-(Ni,Fe)OOH	281	-	Energy Evnviron. Sci,2020, 133439-3446.
Co-NiFe LDH	290	-	Appl. Catal. B, 2022, 314121491.
NiFeOOH/NiFe LDH	290	-	Matter, 2020, 32124-2137
(Ni_7Fe_3)OOH-S	298	-	Chem. Eng. J., 2023, 454, 140030.
NiFe-LDH/N-doped Co/NF	252	262	Nano Res., 2025, 18, 94907190.
$NiFeCoZn^{vac}$-LDH	222	254	Chem. Eng. J., 2025, 508, 161153.
Gd-NiFeLDH@NF	234	270	Small, 2025, 21, 2409265.
NiFeCe-LDH@CP	232	267	Chem. Eng. J., 2023, 464, 142669.
NiFe V/NF	-	263	Appl. Catal. B: Environ. Energy, 2024, 356, 124259.
NiFe-LDH/MOF	-	275	Nano Res., 2023, 16, 8945-8952.
Ag@FeCoNi-LDH@CF	-	207	Int. J. Hydrogen Energy, 2024, 61, 603-610.
d-NiFe-LDH	-	200	Angew. Chem. Int. Ed. 62 (2023) 202217815.
NiFeOOH	-	213	Appl. Catal. B Environ. 341 (2024) 123297.
$(Ni, Fe)_3S_2$/NFF	-	242	Adv. Funct. Mater., 2024, 34, 2400979.
NiFeW LDH	-	247	Chem. Eng. J., 2021, 426, 130768.
$Fe_{17.5\%}$-Ni_3S_2/NF	-	249	ACS Catal., 2018, 8, 5431-5441.
Ni/Fe LDH-Ni_3S_2	-	280	J. Mater. Chem. A, 2023, 11, 19578-19590.
NiFe-Ce LDH	-	220	ACS Nano 2025, 19, 35, 31915–31928

Table S2. Calculated formation energies of oxygen vacancy (E_{OV}) at different sites

	E_{OV} / eV	E_{defect} / eV	E_{OH} / eV	$E_{perfect}$ / eV
NiFe LDH	1.38	-470.67	-10.84	-482.89
Ce site / Ce, Gd-NiFe LDH	0.67	-481.13	-10.84	-492.64
Gd site / Ce, Gd-NiFe LDH	0.97	-480.83	-10.84	-492.64

Table S3. ICP-OES results of electrolyte after stability test

	Ce, Gd-NiFe LDH	Ce-NiFe LDH	Gd-NiFe LDH
Initial mass of electrode / mg	0.0276	0.0231	0.0224
Dissolved amount of Ce / mg	0.000310	0.000365	
Dissolved amount of Gd / mg	0.000099		0.000342

[1] Kresse G, Furthmüller J. Efficiency of ab-initio total energy calculations for metals and semiconductors using a plane-wave basis set[J]. *Computational Materials Science*, 1996, 6(1): 15-50.

[2] Perdew J P, Burke K, Ernzerhof M. Generalized Gradient Approximation Made Simple[J]. *Physical Review Letters*, 1996, 77(18): 3865-3868.